

ISTITUTO NAZIONALE FISICA NUCLEARE

INFN/AE - 79/5

24 dicembre 1979

R. Birsa, F. Bradamante, S. Dalla Torre, M. DI Drusco, M. Giorgi,
K. Kuroda, A. Michalowicz, P. Moras, A. Penzo and P. Schiavon

THE RESPONSE OF ORGANIC SCINTILLATORS AS TARGETS SENSITIVE TO
SLOW PROTON RECOILS MEASURED BY NEUTRON SCATTERING

263

THE RESPONSE OF ORGANIC SCINTILLATORS AS TARGETS SENSITIVE TO
SLOW PROTON RECOILS MEASURED BY NEUTRON SCATTERING

R. Birsa, F. Bradamante, S. Dalla Torre, M. Di Drusco, M. Giorgi,
P. Moras, A. Penzo, P. Schiavon

Istituto di Fisica dell'Università e INFN, Sezione di Trieste
Trieste, Italy

K. Kuroda, A. Michalowicz

Laboratoire de Physique des Particules (LAPP)
Annecy, France

ABSTRACT

With the purpose of studying the performance of a recoil-sensitive scintillation target for high energy applications, the response of plastic and liquid scintillators to proton recoils with energies between 1 and 10 MeV, has been measured in neutron scattering by identifying elastic events with a time-of-flight spectrometer for the scattered neutrons.

1. - INTRODUCTION

Targets made of scintillating organic materials, coupled to a photomultiplier (scintillator target: ST) have been employed at low energies (1-100 MeV), mainly in neutron scattering measurements ¹⁾, to detect slow recoil particles, thus providing information on

- a) occurrence of a neutron interaction in the target,
- b) start for time-of-flight (TOF) measurement to determine the scattered neutron energy,
- c) energy of the recoiling particle.

Furthermore, when using special liquid scintillators, the recoil particle can be identified by pulse shape discrimination (PSD) ²⁾.

Analogously ST have also been successfully employed in elastic scattering of charged pions on deuterium and hydrogen at intermediate energies ³⁾ (100-300 MeV), in the study of coherent diffractive excitation of carbon nuclei by charged high energy pions and protons ⁴⁾ up to 40 GeV, to reduce incoherent background by pulse height analysis.

It has been proposed ⁵⁾ to use a ST detector also as a proton target to detect low energy (1-10 MeV) recoils in pp elastic scattering at small angles ($3 \times 10^{-3} \leq |t| \leq 10^{-2} \text{ GeV}^2$) at very high energies (100-400 GeV), where the identification of elastic events is increasingly difficult on the basis of momentum and angle measurements for the scattered particle alone.

Such a detector would have some advantages compared with gaseous targets associated with ionization, proportional or semiconductor detectors, already employed at high energies ⁶⁾: simpler construction and operation, larger hydrogen density and rate capability.

This last property is particularly important in view of the specific interest of measuring the polarization asymmetry in pp elastic scattering in the Coulomb-nuclear interference region⁷⁾, as a rapid method for calibration of the degree of polarization in a high energy proton beam⁸⁾.

There are however also some obvious difficulties: the light pulse produced in the ST by the incoming and outgoing (charged) fast particles is superimposed to the signal of the recoiling particle and the presence of carbon nuclei is a source of background, which adds up to the inelastic interactions in pure hydrogen.

The first disadvantage can be reduced by adequately segmenting the ST thickness (multiscintillator target: MST) in such a way that the energy deposited by the through-going particles in each counter is a negligible fraction of the energy dissipated by the stopping recoil which is scattered at about 90° in the laboratory; the main background due to elastic scattering on carbon (inelastic processes are quite reduced in the kinematical region of interest owing to the small momentum transfers involved) can be rejected on the basis of the much smaller nuclear recoil energy.

A direct appreciation of the performances of a MST detector can be obtained by testing this technique separately in a low energy neutron beam to study the response for slow proton recoils and in a high energy charged beam to investigate the effects of through-going particles and background events.

In this report we describe measurements performed at the Cockroft-Walton accelerator of the Istituto di Fisica dell'Università di Trieste, in order to determine the response of NE 102 (plastic) and NE 213 (liquid) scintillators* to protons with energies between 1 and 10 MeV.

*)

Produced by Nuclear Enterprises, Inc., Edinburgh - Scotland.

2. - EXPERIMENTAL METHOD AND APPARATUS.

Recoil protons with energies in the interval from 1 to 10 MeV were produced in elastic scattering of 14.2 MeV neutrons on hydrogen contained in organic scintillators; elastic events with neutrons scattered through angles between 15° and 60° in the laboratory were simultaneously identified by detecting the scattered neutron direction and TOF in a second counter.

The pulse height of the recoil proton in the target counter was associated with the kinematically determined proton energy to evaluate the response characteristics of the scintillator: it is well known that quenching effects⁹⁾ tend to reduce the light yield for heavily ionizing particles; it is therefore necessary to calibrate the response as a function of the energy deposited by the particle, to determine the practical lower limit for efficient detection and the pulse height resolution.

Our method is characterized by the possibility of measuring simultaneously all recoil energies between 1 and 10 MeV with on line computer for fast data acquisition and event selection, allowing to rapidly collect large statistical samples of clean elastic np events. By this method it is also possible to measure the differential cross-section for elastic np scattering with short experimental runs, independent on possible point-to-point systematic errors.

The arrangement of the experimental apparatus for the measurement is shown in Fig. 1.

The 200 KeV deuteron beam from the accelerator impinging on a tritium target, produced neutrons by the reaction $T(d,n)\alpha$ and a collimated, monoenergetic 14.2 MeV neutron beam (see Table 1) was defined by tagging the associated α particles in a small ($25 \times 25 \text{ mm}^2$) scintillator detector (A in Fig. 1) set at 85° with respect to the direction of the primary deuteron beam.

Neutrons in the secondary beam interacted in the scintillator target T, positioned 50 cm from the center of the tritium target at an angle of 85° (defined with a resolution of $\pm 5^\circ$ by the A counter acceptance) with respect to the direction of the primary deuteron

beam: two different scintillators, coupled to a XP2020 photomultiplier via an air light guide, were used during the measurement; their characteristics and dimensions are listed in Table 2.

Scattered neutrons were detected in counter N, made of a NE102 scintillator block (120 cm long, with a square cross-section of 5 cm side) placed in the horizontal plane defined by the deuteron beam direction and the target counter center, at a distance d of 1.5 m from 15° to 60° with respect to the neutron beam axis, joining the center of the tritium and scintillating targets. (See Table 3)

The N counter was coupled at both ends to a 56 AVP photomultiplier; the signals from the two tubes gave two independent measurements of the scattered neutron TOF plus light propagation time to the photocathodes, thus allowing to determine the kinematics of individual events by associating the scattered neutron energy obtained by TOF with its scattering angle, obtained from the impact point on the scintillator. With reference to Fig. 1 the two experimental quantities, τ (neutron TOF) and x (distance with sign from the center of N counter of the neutron impact point) are obtained as functions of τ_R and τ_L , the measured overall times of the L and R signals:

$$\begin{aligned} \tau &= \frac{\tau_R + \tau_L}{2} + \tau_0 \\ x &= \frac{v}{2} (\tau_L - \tau_R) \end{aligned} \quad (1)$$

The constants τ_0 and v have been accurately estimated by calibrating the N counter in the direct neutron beam at the position of T counter.

The kinematical quantities E_n and θ_n are obtained from (1) approximately as

$$\begin{aligned} \theta_n &\approx \theta_N - \arctg \frac{x}{d} \\ E_n &\approx \frac{m_p}{2c^2} \left(\frac{d}{\tau \cos \theta_n} \right)^2 \end{aligned} \quad (2)$$

3. - THE ELECTRONICS AND ACQUISITION SYSTEM

Fig. 2 is a block diagram of the electronic apparatus used for the measurement.

For all counters the anode signal was formed out in parallel on two 50 Ω matched outputs: one was fed into a constant-fraction-timing discriminator (CFD)^{*} to generate fast, low slewing logic signals for the trigger, and the second was sent to an ADC circuit for pulse height analysis.

The trigger for the acquisition system was typically given by a coincidence L·R·A·T defining scattering events produced by neutrons with definite direction and energy (A), scattering in the scintillator target (T) into the N counter (L·R); a fraction of the data was also collected with counter T out of the trigger, to estimate the background of events without requirement of a minimum recoil energy. L and R counters were coincided in a Mean-Timer circuit MT, thus giving a signal dependent in time only on the TOF of the scattered neutron and independent of the impact position in the long N counter.

At the occurrence of a trigger signal the information of the time-of-flight and pulse amplitude was read into TDC and ADC CAMAC modules^{**} and transferred to a 2100S HP computer; the start signal for TDC was given by the A counter, gated by L·R·T, while stop signals were driven by L,R and MT pulses: the first two were used for later analysis, while the last one was employed for control only.

The ADC was gated by the trigger signal and stored the T pulse.

Three scales counted the rates of A,A·T and A·T·(L·R). The information was buffered in the computer and recorded on tape (see flow chart in Fig. 3) for normalization purposes in the off-line analysis.

About 40 thousands events have been used for both scintillators to study the response characteristic; also the cross-section has been evaluated on the basis of this statistical sample, collected in about 12 hours: a more detailed description of the acquisition system is given in Ref. 10).

* Ortec Model: 463

** Le Croy Model: 2228A, 2243A

4. - EVENT SELECTION AND ANALYSIS

An interactive program similar to the data acquisition program was used for the off-line analysis of the collected data.

The first part of the analysis consisted in the identification of elastic $np \rightarrow np$ scattering events on the basis of the measured TOF τ_L and τ_R : possible competing reactions are mainly elastic scattering on Carbon $nC \rightarrow nC$ and excitation of the carbon nucleus $nC \rightarrow nC^*$ (4.43 MeV). For the above mentioned reactions the recoil particle energy and the differential cross-section (integrated over the azimuthal acceptance of N counter) as functions of the scattered neutron polar angle θ , are listed in Table 4.

The scatter plot of the measured quantities τ_R and τ_L in the plane (τ_L, τ_R) for events with full trigger L·R·A·T and without requiring the signal of the target counter, L·R·A, are respectively shown in Fig. 4 and Fig. 5.

The experimental points are contained in a band whose widths for $\tau_L = \text{const.}$ and $\tau_R = \text{const.}$ are equal, corresponding to the double of light transit time through the entire N counter scintillator length. The curves superimposed correspond to the expected loci τ_L, τ_R for the three relevant reactions. The recoil proton kinetic energy E_p can be considered as a parameter of the curve corresponding to np elastic scattering. If $\tau_L'(E_p)$ and $\tau_R'(E_p)$ represent the point of the curve corresponding through kinematics to E_p , the quantity

$$(3) \quad X^2 = [\tau_L - \tau_L'(E_p)]^2 + [\tau_R - \tau_R'(E_p)]^2$$

has a χ^2 distribution (a part from a scale factor), since the variances for the measured τ_L and τ_R are the same ($\sigma_L \approx \sigma_R \approx \sigma_\tau = 1 \text{ nsec}$), and τ_L and τ_R can be considered as uncorrelated, due to the negligible slewing of CFD timing. It can therefore be conveniently used to test the hypothesis of an elastic np scattering.

To each event point (τ_L, τ_R) is associated the value E_p such that X^2 is minimum: $X^2 = \tilde{X}^2$. The distribution of \tilde{X} (square root with sign of \tilde{X}^2) for np scattering events with $1 \leq E_p \leq 10 \text{ MeV}$, on NE 213 scintillator, is shown in Fig. 6: for the properties of χ^2 distributions with 1 degree of freedom, \tilde{X} behaves as a gaussian variable centered at zero with variance σ_τ^2 .

The resolution σ_{E_p} , in the kinematically determined recoil proton kinetic energy E_p is listed in Table 5; for events with $|\tilde{X}| \leq 2\sigma_\tau$ and $1 \leq E_p \leq 9$ MeV the target counter T amplitude distributions of 8 bins of E_p , 1 MeV wide, have been obtained; in Fig. 7 and Fig. 8 are shown the distributions for three bins of E_p in the targets of NE 213 and NE 102 respectively.

5. - RESULTS

Comparison of the scatter plots in Fig. 4 and Fig. 5 clearly shows the suppression of background, particularly from carbon scattering, obtained by requiring a target signal above a specified threshold.

Clean elastic events under the peak in the distribution of pulse height H_T from the target counter in each E_p bin (after subtraction of the residual background estimated from the channel content out of the peak) have been used to estimate the cross-section for np scattering at 14.2 MeV, shown in Fig. 9; also data from other measurements^{11),12)} are drawn. Our data have been normalized at 30° with previous values from ref. 11); a normalization based on the integrated rate measured by counter A agrees within few percent.

The dependence on the mean values $\langle H_T \rangle$ for the pulse height distributions in the two scintillator targets of the recoil energy E_p is shown in Fig. 10 and Fig. 11, displaying a loss of scintillation efficiencies at low proton energies, due to quenching effects. This dependence was also checked with a monitor counter at fix angles.

The calibration factor $Q = H_T/E_p$ for each bin in E_p has a distribution with mean value \bar{Q} and variance σ_Q^2 ; the ratios Q/\bar{Q} for both scintillators are listed in Table 6 versus the corresponding E_p value.

It seems that the NE 102 scintillator would give better resolution in the determination of the recoil proton energy: however the liquid NE 213 scintillator has PSD properties which could be exploited as described in Ref. 5.

6. - CONCLUSIONS

With the experimental arrangement described in this report it has been possible to deposit accurately controlled amounts of energy uniformly over the whole volume of scintillator detectors to determine their response; recoil protons with energy as low as 1 MeV can be accurately detected with good resolution.

With the same facility a detailed study of the PSD properties for various liquid scintillators is in progress; a prototype MST has also been tested in a charged high energy beam.

Results of this test, combined with those described in this report show the feasibility of a full size MST for pp elastic scattering at very high energies.

ACKNOWLEDGEMENTS

G. Menon, G. Maselli and J. Lemarec have valuably contributed to the preparation and installation of the apparatus. G. Kidric and F. Tomasini took care of the smooth operation of the accelerator. Two of us express their thanks to the Director of the Istituto di Fisica dell'Università di Trieste Prof. G. Poiani for hospitality at the Institute. Prof. F. Demanins has given valuable suggestions and support.

R E F E R E N C E S

1. - J.T. Lindow et al., Nucl. Instr. Meth. 85 (1970) 151.
R. Madey and F.M. Waterman, Nucl. Instr. Meth. 106 (1973) 89.
G.R. Norman et al., Nucl. Instr. Meth. 100 (1972) 77.
2. - F.D. Brooks, Nucl. Instr. Meth. 4 (1959) 151.
L.M. Bollinger and G.E. Thomas, Rev. Sci. Instr. 32 (1961) 1044.
3. - K. Gabathuler et al., Nucl. Phys. B55 (1973) 397.
4. - W. Melhop et al., Proc. Topical Seminar on High-energy collisions involving nuclei, Trieste (1974). (Editrice Compositori, Bologna, 1975) p. 85.
P.L. Frabetti et al., Nucl. Phys. B158 (1979) 57.
5. - K. Kuroda et al., On the possibility of using a multiscintillator target for small angle elastic scattering at high energies, EP Int. Rep. 79-1 (17 January 1979).
6. - A.A. Vorobyov et al., Nucl. Instr. Meth. 119 (1974) 509.
V. Bartenev et al., Phys. Rev. Lett. 31 (1973) 1088.
T. Ekelof, Low-energy recoil measurements in high-energy physics, Yellow Report CERN 76-23 (1976).
7. - R. Birsa et al., Calibration and monitoring of a high-energy polarized proton beam by asymmetry measurements in the Coulomb-interference region of proton-proton elastic scattering (in preparation).
8. - A. Apokin et al., Study on spin effects at SPS energies using a polarized proton beam, CERN/SPSC/77-61/P 87 (1977).
I.P. Auer et al., Construction of polarized beams and an enriched antiproton beam facility in the Meson Laboratory and experiments using such a facility, Fermilab Proposal N°581 (27 January 1978).
9. - G. Laustriat, The luminescence Decay of organic scintillators, Proc. International Symposium on Organic Scintillators, Argonne Nat. Lab. June 1966 (Ed. D.L. Harrocks) (Gordon and Breach N.Y.) (1968), 127.
10. - M. Di Drusco, Studio della fisica connessa con i fasci di protoni polarizzati ad alte energie e progetto di un polarimetro per la misura della polarizzazione degli stessi (thesis).
11. - A. Suhami and R. Fox, Phys. Lett. 24B (1967) 173.
12. - J.C. Allred et al., Phys. Rev. 91 (1953) 90.
13. - R.J. Howerton, Tabulated Differential Neutron Cross-section UCRL - 55 - 73 - 3rd part - Vol. 1 (1961).

θ_{α}	θ_n	T_n
(degrees)	(degrees)	(MeV)
80.00	90.50	14.10
82.50	87.95	14.14
85.00	85.42	14.18
87.50	82.90	14.22
90.00	80.41	14.27

TABLE 1 - Kinematical quantities relevant to the reaction $T(d,n)\alpha$ at 200 KeV.

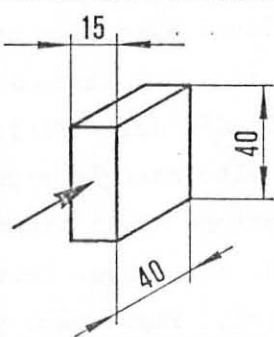
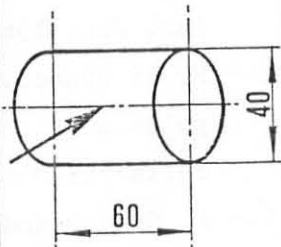
TARGET TYPE	NE 102	NE 213
Density (g/cm^3)	1.032	0.874
Light output (% Anthracene)	65	78
Decay time. (nsec)	2.4	3.7
Wavelength of max. emission (\AA)	4'230	4'250
Atomic ratio H/C	1.104	1.213
Shape and dimensions (mm)		

TABLE 2 - Characteristics and dimensions of the scintillating targets.

θ_n	T_n	spec. TOF _n	θ_p	T_p
(degrees)	(MeV)	(nsec/m)	(degrees)	(MeV)
14.93	13.25	20.1	74.95	0.95
19.92	12.54	20.6	69.93	1.66
24.90	11.66	21.4	64.92	2.54
29.88	10.65	22.3	59.91	3.55
34.87	9.53	23.6	54.90	4.67
39.86	8.33	25.2	49.89	5.87
44.85	7.10	27.3	44.89	7.10
49.84	5.87	30.0	39.89	8.33
54.84	4.67	33.6	34.90	9.53
59.84	3.55	38.5	29.91	10.65

TABLE 3 - Kinematical quantities relevant to np elastic scattering at 14.2 MeV.

θ_n	n + p → n + p		n + C → n + C		n + C → n + C*	
	T_p	$\frac{d\sigma}{d\theta}$	T_C	$\frac{d\sigma}{d\theta}$	T_{C^*}	$\frac{d\sigma}{d\theta}$
(degrees)	(MeV)	($\frac{\text{mbarn}}{\text{rad}}$)	(MeV)	($\frac{\text{mbarn}}{\text{rad}}$)	(MeV)	($\frac{\text{mbarn}}{\text{rad}}$)
17.4	1.28	6.4	0.17	15.7	.13	2.3
22.4	2.08	6.3	0.25	13.0	.19	1.9
27.4	3.03	6.2	0.36	10.3	.26	1.4
32.4	4.10	6.0	0.48	6.9	.35	1.1
37.4	5.26	5.7	0.60	4.5	.45	0.9
42.4	6.48	5.2	0.75	3.4	.55	0.9
47.4	7.72	4.8	0.90	2.4	.67	0.8
52.4	8.94	4.2	1.05	1.4	.80	0.8

TABLE 4 - Comparative table of kinematical parameters and cross-sections (integrated over azimuthal acceptance of N counter) for reactions np→np, nC→nC, nC→nC* (4.43 MeV) at 14.2 MeV (Ref. 13)

E_p (MeV)	σ_{E_p} (MeV)	σ_{E_p} / E_p
1.5	0.6	0.40
2.5	0.6	0.24
3.5	0.5	0.14
4.5	0.4	0.09
5.5	0.3	0.05
6.5	0.25	0.04
7.5	0.2	0.03
8.5	0.2	0.02

TABLE 5 - Resolution for E_p as obtained from measured τ_L and τ_R through kinematics.

E_p	σ_Q / \bar{Q} (NE 213)	σ_Q / \bar{Q} (NE 102)
(MeV)		
1 to 2	0.32	0.19
2 to 3	0.24	0.19
3 to 4	0.22	0.18
4 to 5	0.19	0.13
5 to 6	0.15	0.10
6 to 7	0.14	0.06
7 to 8	0.12	0.06
8 to 9	0.10	0.05

TABLE 6 - Ratio of σ_Q and \bar{Q} versus E_p . The energy E_p is obtained from τ_L and τ_R .

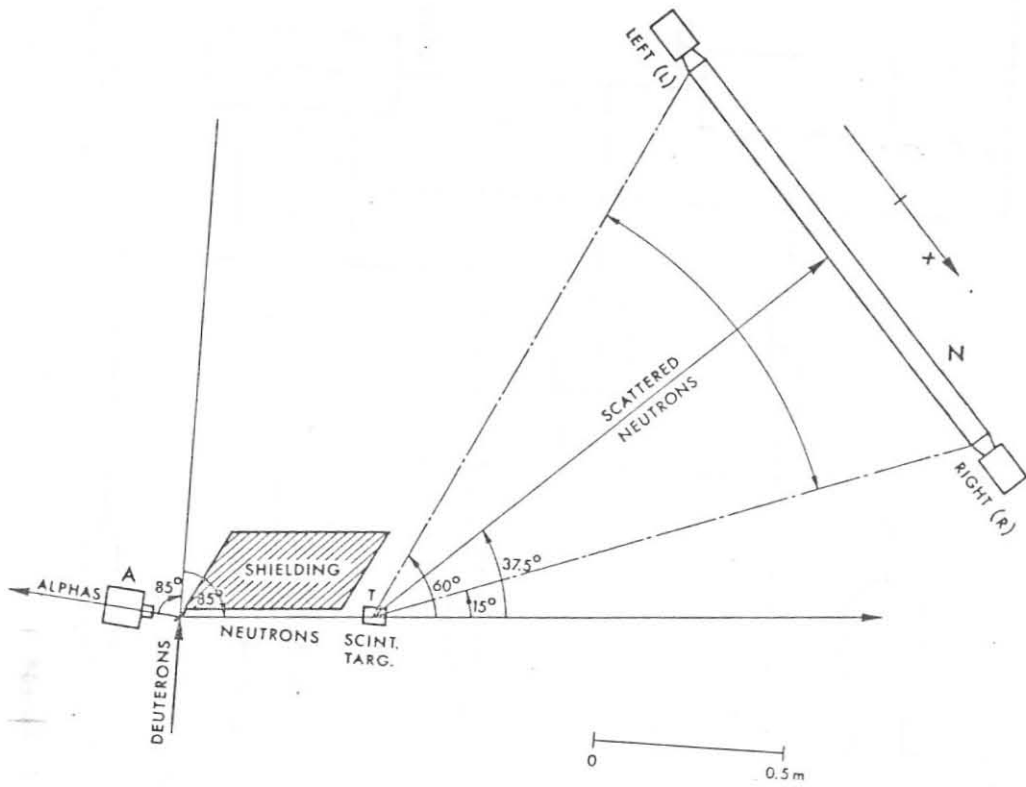


Fig. 1 - Experimental apparatus.

278

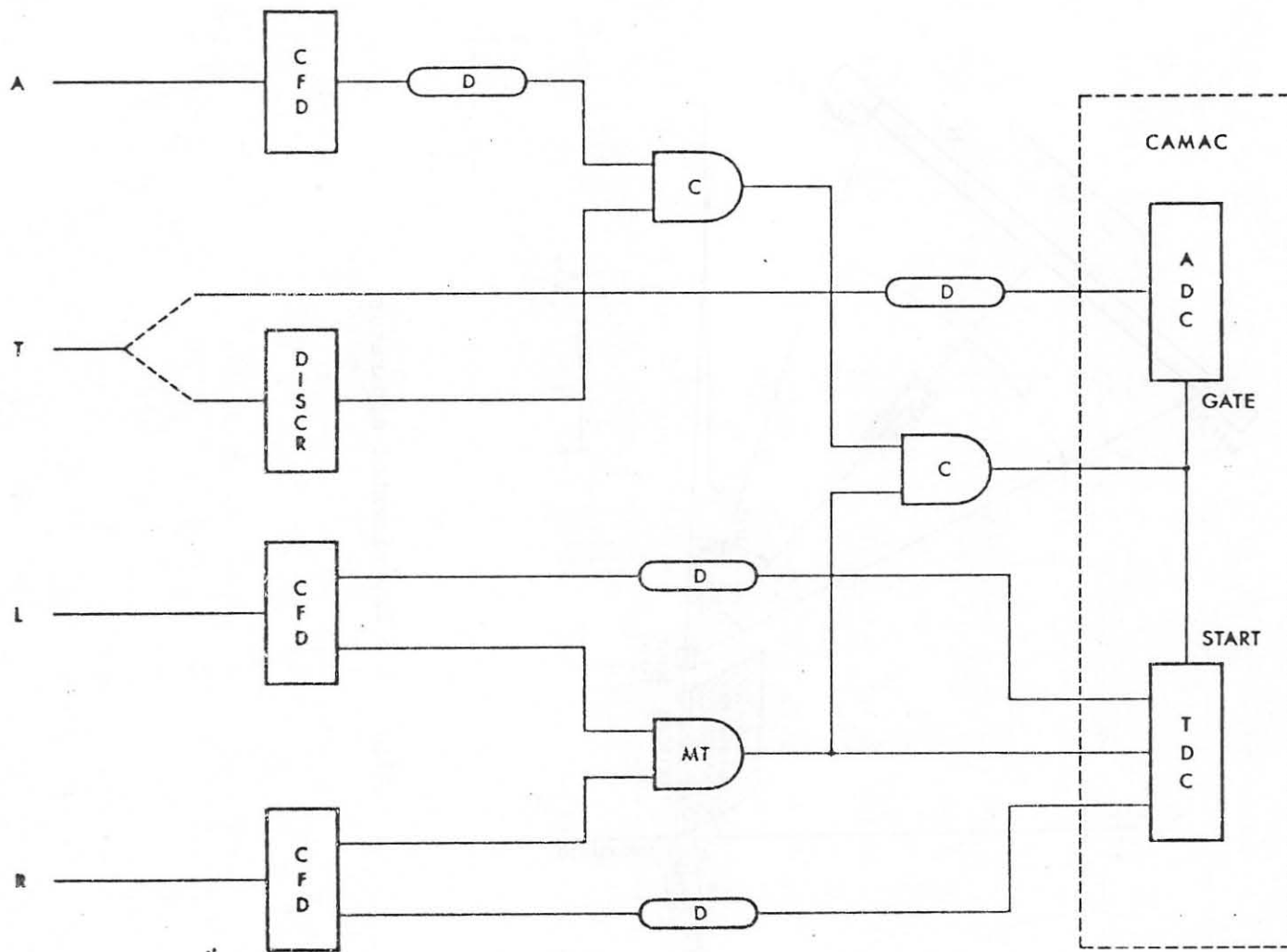


Fig. 2 - Electronics' block diagram.

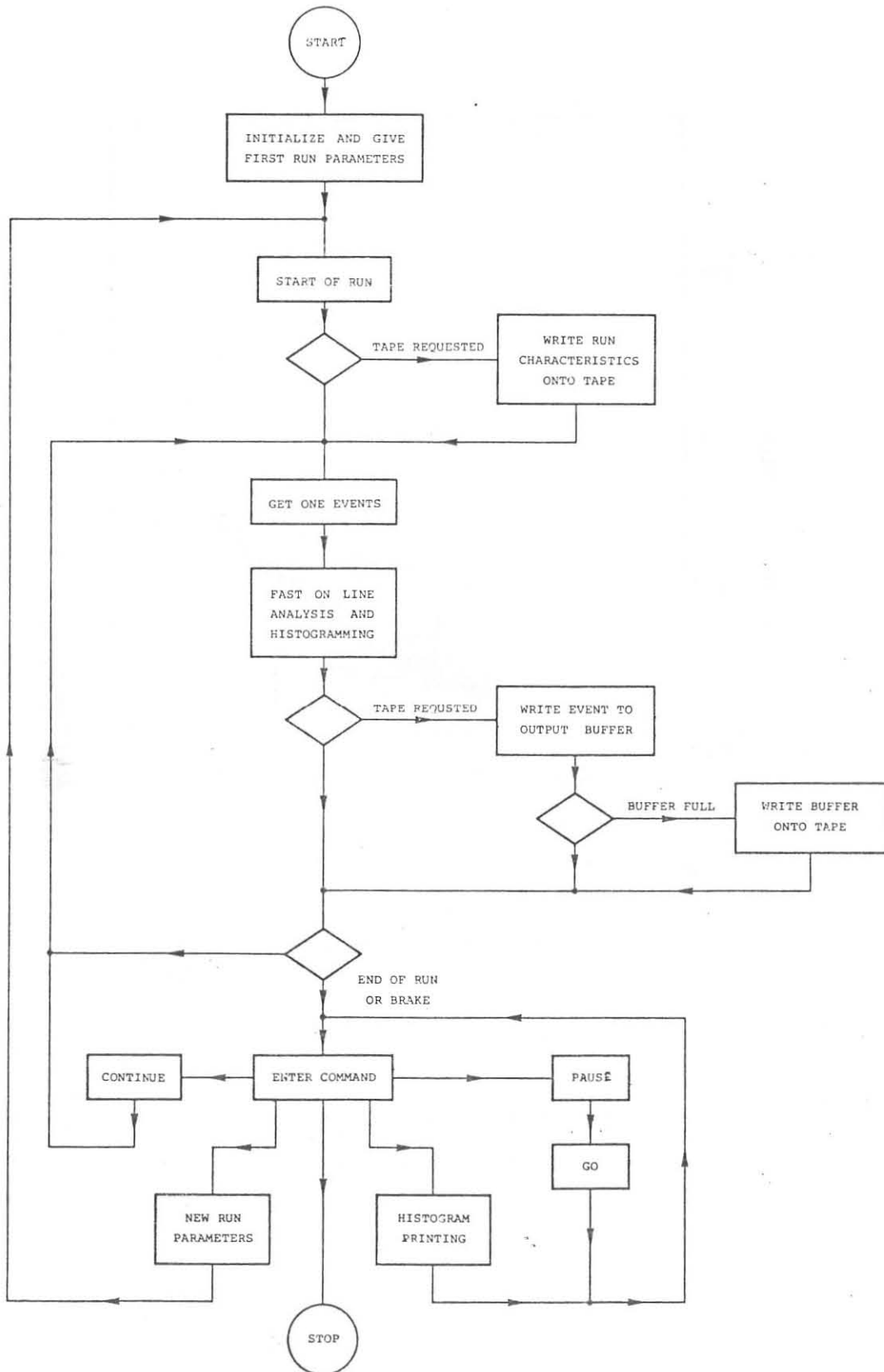


Fig. 3 - Flowchart of the data acquisition program.

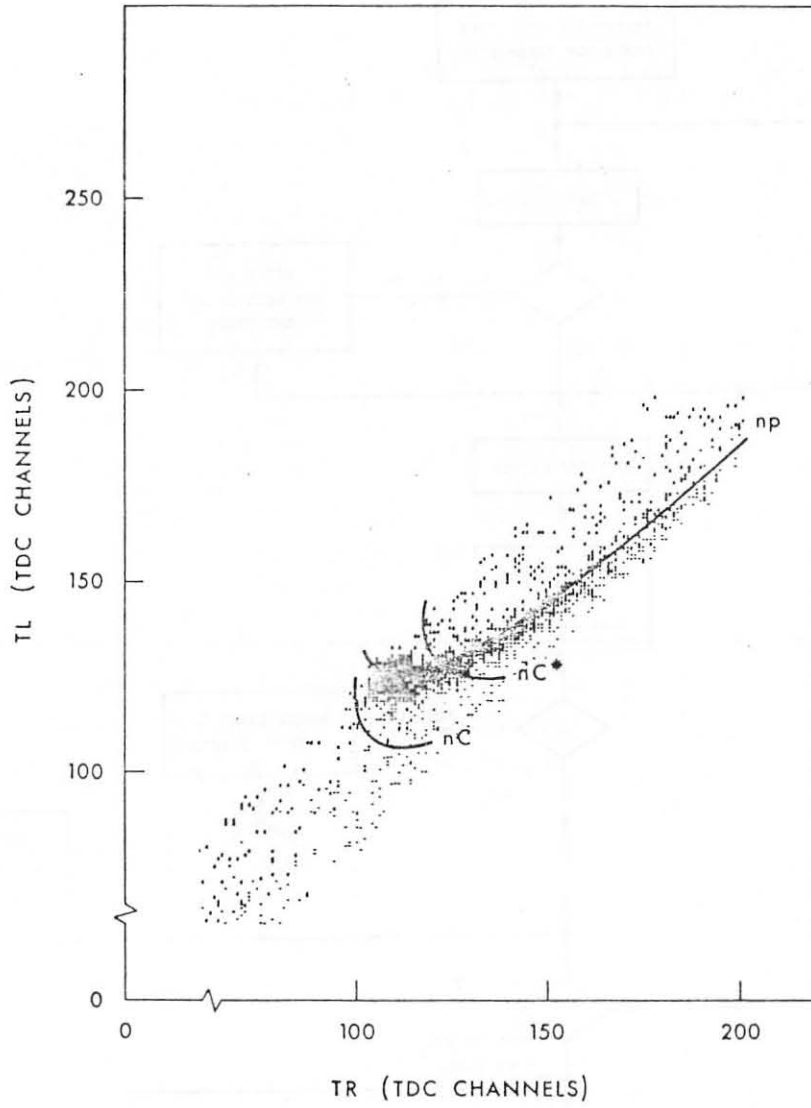


Fig. 4 - Distribution of experimental points (τ_R, τ_L) for events with trigger L·R·A·T (2000 events).

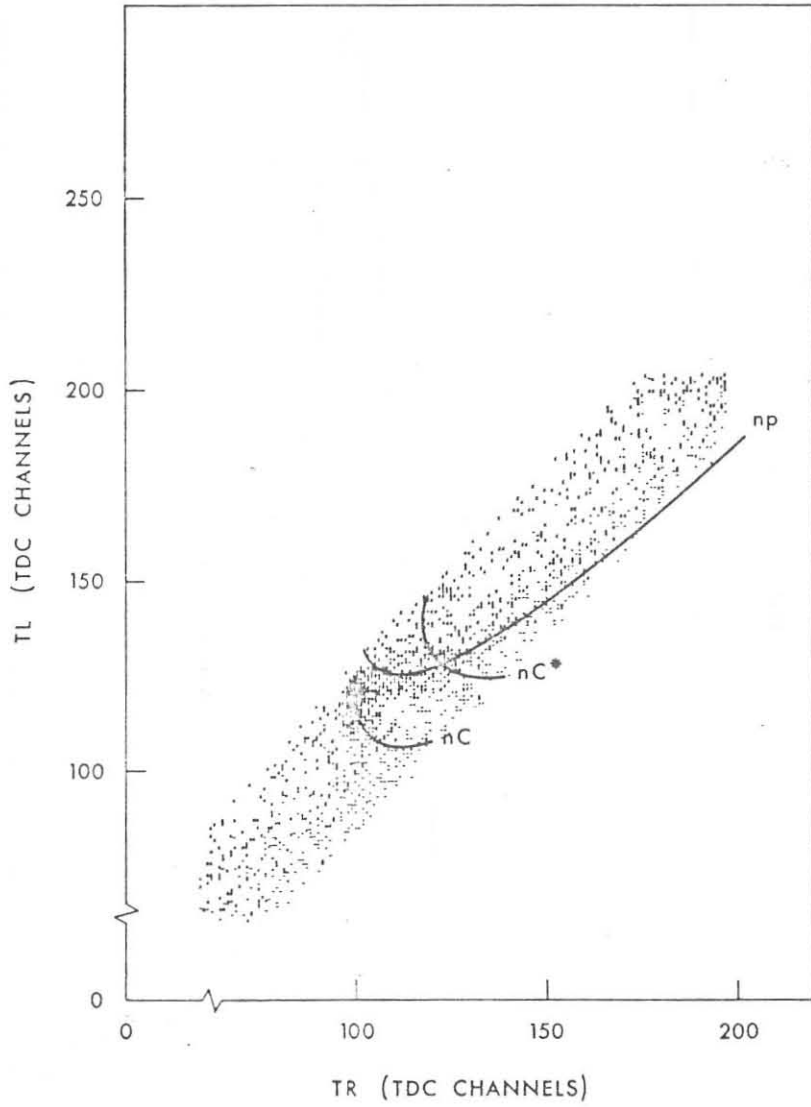


Fig. 5 - Distribution of experimental points (τ_R, τ_L) for events with trigger L.R.A.(2000 events).

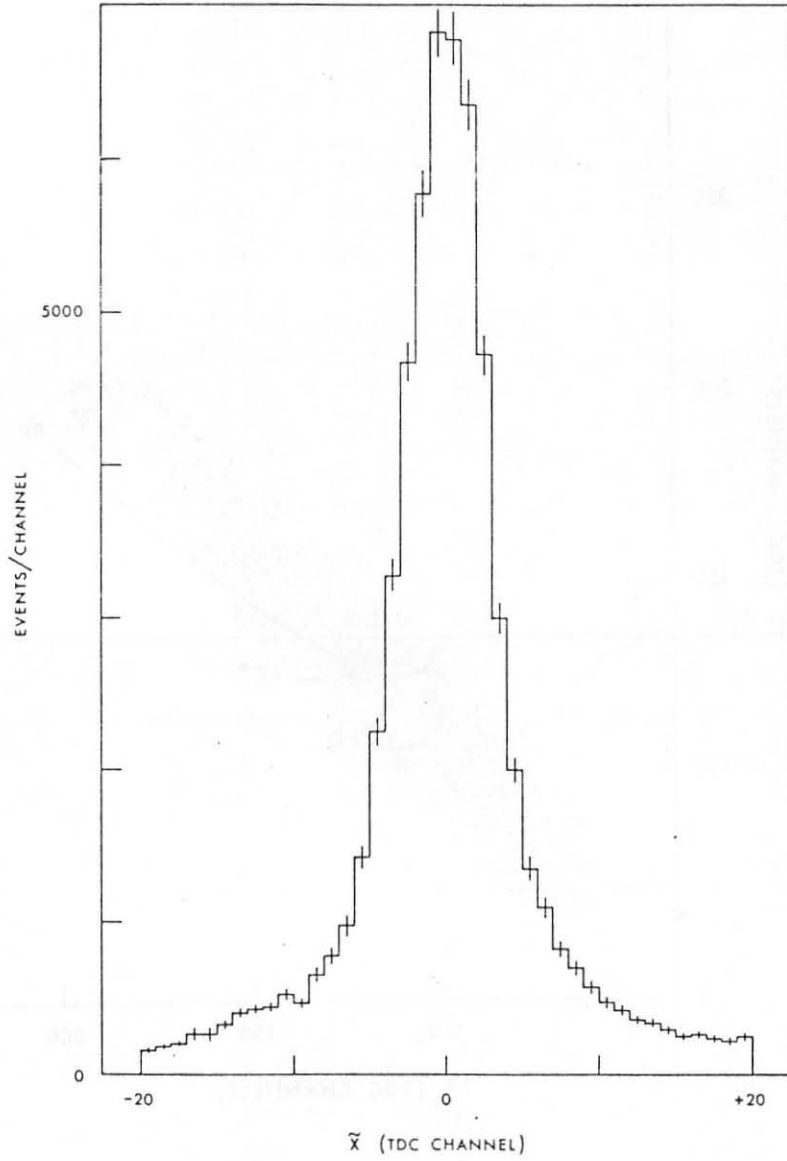


Fig. 6 - Distribution of \tilde{X} variable for scattering events on NE 213 with $1 \leq E_p < 9$ MeV (40000 events).

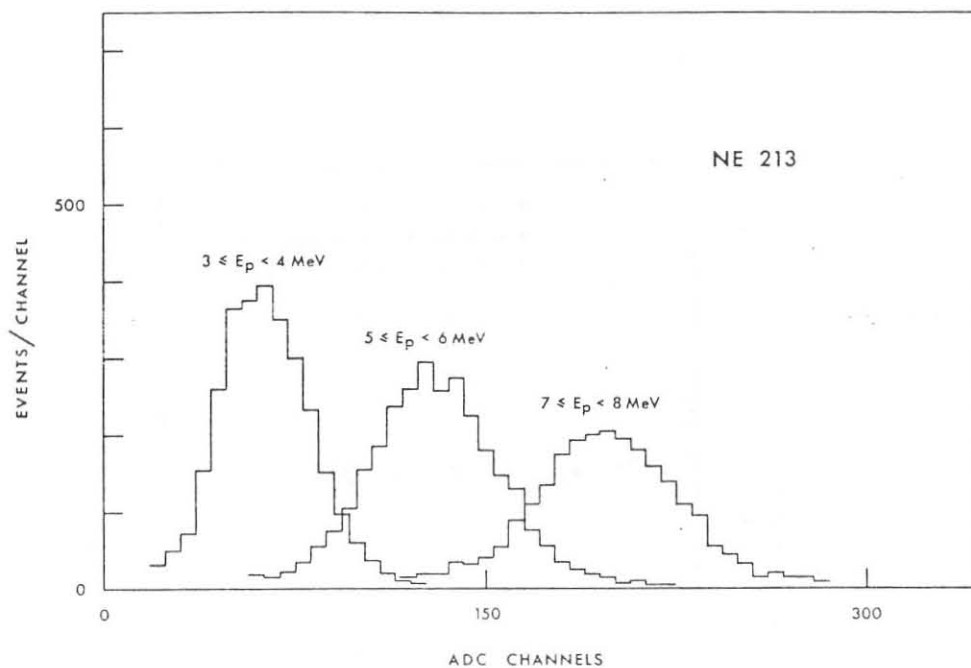


Fig. 7 - Target pulse amplitude distribution in NE 213 for events with $|\tilde{X}| \leq 2\sigma_\tau$ in three E_p bins (10000 events).

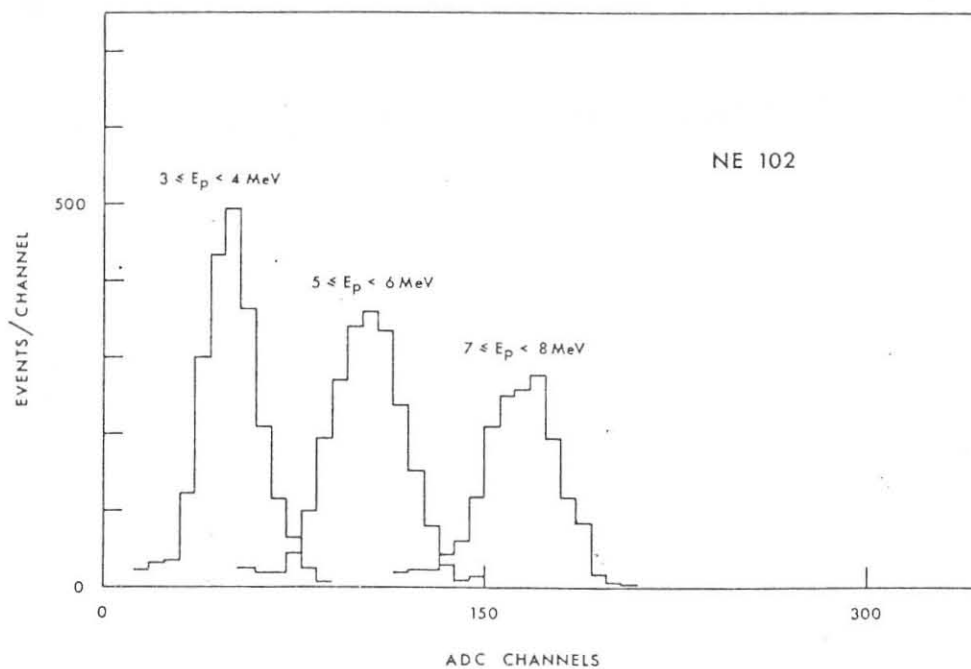


Fig. 8 - Target pulse amplitude distribution in NE 102 for events with $|\tilde{X}| \leq 2\sigma_\tau$ in three E_p bins (7200 events).

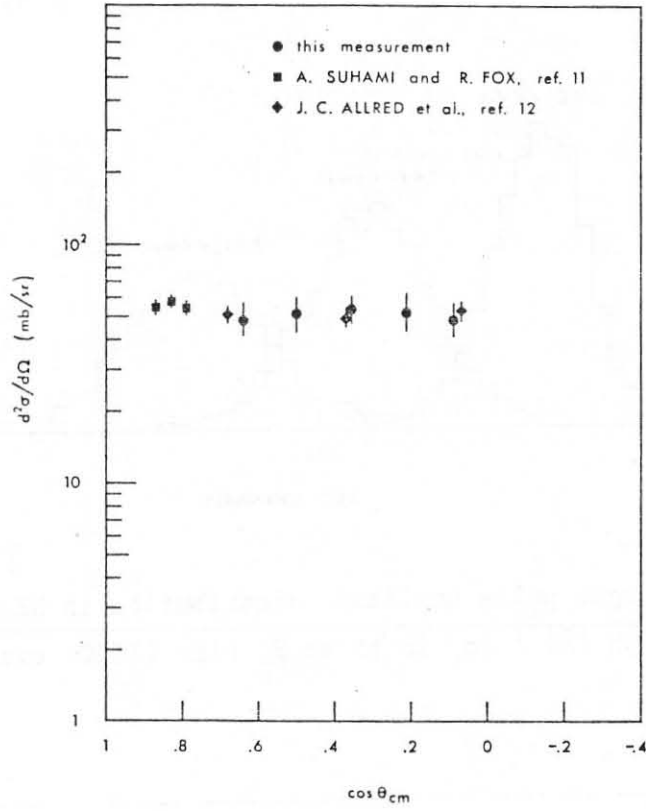


Fig. 9 - Differential cross-section for np elastic scattering at 14.2 MeV.

285

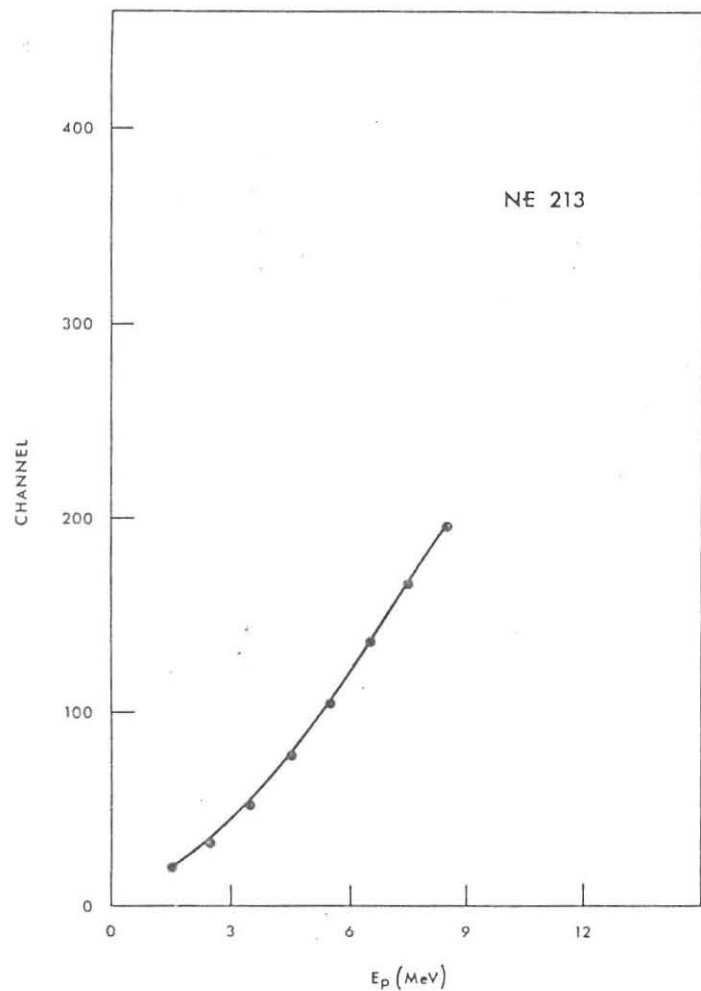


Fig. 10 - Mean values of target pulse amplitude spectra versus E_p for NE 213.

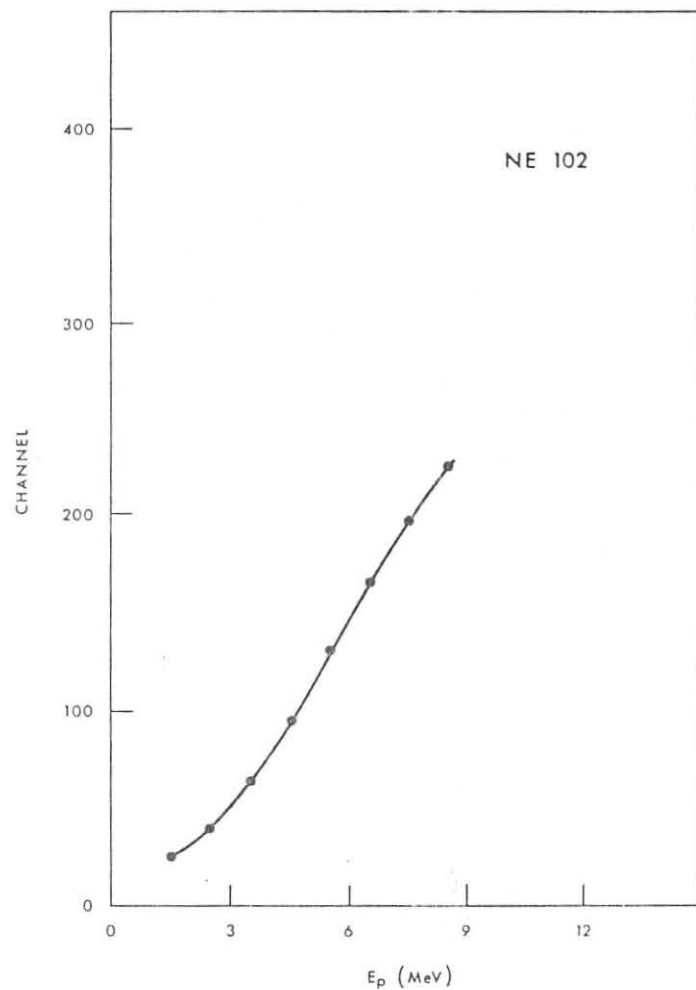


Fig. 11 - Mean values of target pulse amplitude spectra versus E_p for NE 102.